Intramolecular Electron Transfer versus Substrate Oxidation in Lactoperoxidase: Investigation of Radical Intermediates by Stopped-Flow Absorption Spectrophotometry and (9−285 GHz) Electron Paramagnetic Resonance Spectroscopy†

Alistair J. Fielding,‡ Rahul Singh,‡ Barbara Boscolo,§ Peter C. Loewen,|| Elena M. Ghibaudi,*,§ and Anabella Ivancich*,‡

CNRS, URA 2096. CEA, IBITEC, Laboratoire de Hyperfréquences, Métalloprotéines et Systèmes de Spin, F-91191 Gif-sur-Yvette, France, Dipartimento di Chimica I.F.M., Università di Torino, Torino, Italy, and Department of Microbiology, University of Manitoba, Winnipeg, MB R3T 2N2, Canada

Received June 2, 2008; Revised Manuscript Received July 22, 2008

ABSTRACT: We have combined the information obtained from rapid-scan electronic absorption spectrophotometry and multifrequency (9−295 GHz) electron paramagnetic resonance (EPR) spectroscopy to unequivocally determine the electronic nature of the intermediates in milk lactoperoxidase as a function of pH and to monitor their reactivity with organic substrates selected by their different accessibilities to the heme site. The aim was to address the question of the putative catalytic role of the protein-based radicals. This experimental approach allowed us to discriminate between the protein-based radical intermediates and [Fe(IV)═O] species, as well as to directly detect the oxidation products by EPR. The advantageous resolution of the *g* anisotropy of the Tyr• EPR spectrum at high fields showed that the tyrosine of the [Fe(IV)═O Tyr•] intermediate has an electropositive and pH-dependent microenvironment [g_x value of 2.0077(0) at pH ≥ 8.0 and 2.0066(2) at 4.0 ≤ pH ≤ 7.5] possibly related to the radical stability and function. Two types of organic molecules (small aromatic vs bulkier substrates) allowed us to distinguish different mechanisms for substrate oxidation. [Fe(IV)═O Por•+] is the oxidizing species of benzohydroxamic acid, *o*-dianisidine, and *o*-anisidine via a heme-edge reaction and of mitoxantrone via a long-range electron transfer (favored at pH 8) not involving the tyrosyl radical, the formation of which competed with the substrate oxidation at pH 5. In contrast, the very efficient reaction with ABTS at pH 5 is consistent with [Fe(IV)═O Tyr•] being the oxidizing species. Accordingly, the identification of the ABTS binding site by X-ray crystallography may be a valuable tool in rational drug design.

Lactoperoxidase (LPO,[1] EC 1.11.1.7) is synthesized in the breast secretory epithelial cells (*1*) and is found in secretions like milk, saliva, and tears (*2*). As in the case of the other members of the mammalian peroxidase family (*3*), the ferric enzyme catalyzes the oxidation of halides and pseudohalides by hydrogen peroxide, the products exhibiting a wide range of antimicrobial activity (*4*). Moreover, the Compound I intermediate formed upon reaction of the ferric (resting) enzyme with hydrogen peroxide is able to oxidize substrates of rather different sizes such as phenols (*5, 6*), catechol(amine)s (*7*−*9*), aromatic amines (*10*−*12*), steroid hormones (*13*−*15*), and polycyclic aromatic hydrocarbons (*16*). The recently deposited X-ray crystal structure of the bovine enzyme at 2.34 Å resolution (PDB entry 2GJ1) confirmed the prediction of a deeply buried heme site with a restrictive substrate access channel (*17*), and the structures of the enzyme in complex with small substrates [thiocyanate (2IPS), 2-hydroxybenzohydroxamic acid (also named salicylhydroxamic acid) (2QPK), and acetylsalycilic acid (2QQT)] revealed a binding site in close contact with the heme iron and the distal-side histidine. Thus, the typical heme-edge reaction through the [Fe(IV)═O Por•+] species is expected for such small substrates, as previously inferred from kinetic studies (*18, 19*). The question about the mechanism for the oxidation of larger substrates that cannot possibly access the heme pocket arises along with the question of whether protein-based radical species are the alternative reactive

† This work was partially supported by the French CNRS and CEA Saclay (to A.I.) and grants from the Natural Sciences and Engineering Research Council of Canada (to P.C.L.) and the Canadian Research Chair Program (to P.C.L.). A.J.F. and R.S. acknowledge postdoctoral fellowships from CEA Saclay.

* To whom correspondence should be addressed. A.I.: Centre d'Etudes de Saclay, iBiTec, SB2SM, Bat. 532, pièce 210 D, 91191 Gif-sur-Yvette, France; phone, +33 1 69 08 28 42; fax, +33 1 69 08 87 17; e-mail, anabella.ivancich@cea.fr. E.M.G.: Dipartimento di Chimica I.F.M., Università di Torino, via Giuria 7, I-10125 Torino, Italy; phone, +39-011-6707951; fax, +39-011-6707855; e-mail, elena.ghibaudi@unito.it.

‡ CNRS.

§ Università di Torino.

|| University of Manitoba.

[1] Abbreviations: LPO, lactoperoxidase; EPR, electron paramagnetic resonance; HF EPR, high-field electron paramagnetic resonance; SDV, singular-value decomposition; BHA, benzohydroxamic acid; SHA, 2-hydroxybenzohydroxamic acid or salicylhydroxamic acid; *o*-anisidine, 2-methoxyaniline; *o*-dianisidine, 3,3′-dimethoxybenzidine; ABTS, 2,2′-azinobis(3-ethylbenzthiazoline-6-sulfonic acid); mitoxantrone, 1,4-dihydroxy-5,8-bis[2-(2-hydroxyethylamino)ethylamino]anthracene-9,10-dione.

10.1021/bi801032k CCC: $40.75
Published on Web 08/20/2008

intermediates as in the cases of lignin peroxidase (*20*) and *Mycobacterium tuberculosis* catalase-peroxidase (*21*) or they are tuned for facilitating electron transfer between the substrate(s) and the active site as in the case of ribonucleotide reductase (*22*).

In lactoperoxidase, indirect evidence of the formation of protein-based radical species as isomers of the [Fe(IV)═O Por$^{\bullet+}$] intermediate has been reported previously (reviewed in ref *23*). Specifically, spin trapping experiments indicated the formation of a protein radical, and mass spectrometry analysis showed that a surface residue, Tyr289, was at the origin of the enzyme dimerization via a dityrosine cross-link (*24*). Kinetic studies of the enzyme reaction with para-substituted phenols using stopped-flow absorption spectrophotometry exhibited very low enzyme reactivity at pH 5 for phenols containing an amino group, and a low-potential Compound II (proposed to be a tyrosyl radical intermediate) was invoked to explain such behavior (*6*). It is of note that the electronic absorption spectrum of the enzyme upon reaction with hydrogen peroxide reflects mostly the changes in electronic structure of the heme iron, since the expected absorption bands for tyrosyl and tryptophanyl radicals (410 and 500−600 nm, respectively) are masked by the heme bands (*25*).

In this work, we have combined the information obtained from rapid-scan electronic absorption spectrophotometry and from multifrequency (9−295 GHz) EPR spectroscopy to unequivocally determine the electronic nature of the reactive intermediates formed in LPO as a function of pH and to monitor their reactivity with organic substrates. The use of lower temperatures (5 °C) to perform the reaction mixtures allowed us to better resolve the oxidation reactions, which at room temperature may happen within the dead time of the stopped-flow instrument. The advantageous resolution of the *g* anisotropy of the Tyr$^{\bullet}$ EPR spectrum at high fields (285 GHz/10 T) showed that the tyrosine being the site for the [Fe(IV)═O Tyr$^{\bullet}$] intermediate has an electropositive and specific pH-dependent microenvironment (most possibly a hydrogen-bond interaction), thus implying a fine-tuned mechanism for the radical stabilization despite the existence of 15 Tyr residues. The choice of substrates with very distinct sizes (small aromatic vs bulkier substrates) allowed us to distinguish between two different mechanisms for substrate oxidation: the heme-edge reaction for the small substrates [benzohydroxamic acid, *o*-dianisidine, and *o*-anisidine, the latter being a carcinogen in the bladder of both rats and mice (*26*)] with [Fe(IV)═O Por$^{\bullet+}$] being the oxidizing species and two different long-range electron transfer mechanisms for the reaction with the bulkier substrates, possibly explained by different binding sites on the surface of the enzyme. Interestingly, while the [Fe(IV)═O Por$^{\bullet+}$] intermediate was the reactive species for mitoxantrone, the very efficient reaction at pH 5 was consistent with [Fe(IV)═O Tyr$^{\bullet}$] being the oxidizing species for ABTS. The ABTS reaction (specific activity and reaction rates) exhibited a very different behavior as a function of pH as compared to the other substrates. Mitoxantrone is a chemotherapy drug used in the treatment of leukemia and breast cancer (*27, 28*). Our findings indicate that the identification of the ABTS binding site by X-ray crystallography may be a valuable tool in rational drug design.

EXPERIMENTAL PROCEDURES

Sample Preparation. LPO was purified from bovine raw milk as previously described (*29*). The enzyme concentration was determined using an extinction coefficient of 114000 M^{-1} cm^{-1} at 412 nm (*29*), and the concentration of hydrogen peroxide (30%, v/v, Sigma-Aldrich) was determined at 240 nm using an extinction coefficient of 39.4 M^{-1} cm^{-1} (*30*). *o*-Anisidine, *o*-dianisidine, mitoxantrone, BHA, and ABTS were purchased from Sigma-Aldrich. To prevent the substantial change in pH of phosphate buffer that occurs on freezing, Tris-maleate (50 mM) buffer was used. Buffer was exchanged using centricon Y10 microconcentrators (Amicon). Taking into account previous reports of modifications of the native enzyme when using Tris buffer (*31*), we compared the ferric EPR signals (recorded at 4 K) of LPO in Tris-maleate buffer at pH 5.2, 7.0, and 8.0 with that of the enzyme in succinate (pH 5.0), HEPES (pH 7.0), and CAPS (pH 10.0) buffers and concluded there was no substantial effect of the Tris-maleate buffer on the rhombicity of the ferric (high-spin) signal at a given pH. The control samples for the ABTS radical in Figure S3 (Supporting Information) were generated by the reaction of 0.4 mM ABTS, 2.5 mM peroxyacetic acid, and 20 nM catalase-peroxidase in a 50 mM buffer solution (sodium acetate for pH 5.2 and phosphate for pH 7.2). This reaction was performed at room temperature for 5 min.

Peroxidase Activity Measurements. Activity measurements were monitored with a UVIKON 922 (Kontron, St. Quentin-en-Yvelines, France) spectrophotometer, equipped with temperature-controlled cell holders and a water circulating bath (Minichiller). ABTS oxidation was followed spectrophotometrically at 405 nm ($\varepsilon = 36.8$ mM^{-1} cm^{-1}) in a final volume of 1 mL, containing 400 μM ABTS, 2.5 mM H_2O_2, and appropriately diluted LPO in 50 mM Tris-maleate at pH 5 and 8. *o*-Dianisidine oxidation was followed at 460 nm ($\varepsilon_{460} = 11.3$ mM^{-1} cm^{-1}) in a final volume of 1 mL containing 350 μM *o*-dianisidine, 100 μM H_2O_2, and appropriately diluted LPO in 50 mM Tris-maleate at pH 5 and 8. *o*-Anisidine oxidation was followed at 450 nm (diimine formation) ($\varepsilon_{450} = 11.3$ mM^{-1} cm^{-1}) and 500 nm (quinone imine formation) ($\varepsilon_{500} = 7.5$ mM^{-1} cm^{-1}) in a final volume of 1 mL containing 700 μM *o*-anisidine, 100 μM H_2O_2, and appropriately diluted LPO in 50 mM Tris-maleate at pH 5 and 8. Activity measurements were performed at 5 and 20 °C to compare with the stopped-flow UV−vis absorption experiments.

EPR Spectroscopy. Conventional EPR spectra were recorded at 9.4 GHz on a Bruker Elexsys E500 spectrometer fitted with a standard TE_{102} cavity equipped with a liquid helium cryostat (Oxford Instruments) and a microwave frequency counter (Bruker ER049X). The home-built high-field EPR spectrometer (95−285 GHz) has been described previously (*32*). The absolute error in *g* values of the 285 GHz EPR spectra was 1×10^{-4}. The relative error in *g* values between any two points of a given spectrum was 5×10^{-5}. Initial protein concentrations of 1.2 mM were used for the EPR spectra shown in Figure 1. Typically, samples were prepared by manually mixing 40 μL of the native enzyme (in 50 mM Tris-maleate buffer for the pH range from 5.2 to 8.6) with an equal volume of a 5-fold excess of a hydrogen peroxide solution (buffered at the same pH as the

sample), directly in the 4 mm EPR tubes kept in ice. The reaction was stopped by rapidly immersing the EPR tube in liquid nitrogen. Different combinations of mixing times (2, 10, and 15 s) with an excess of hydrogen peroxide (5-, 10-, and 15-fold) were used to determine the highest yield of the EPR radical signal as a function of pH. The highest yields were obtained with a 5-fold excess of hydrogen peroxide and a mixing time of 2 s in ice for the enzyme at acidic and neutral pH values, while for basic pHs, the optimal conditions were a 5-fold excess of hydrogen peroxide and a mixing time of 15 s in ice. Spin quantification of the radical signal resulted in 0.4 spin/heme. The 9 GHz EPR experiments for the reaction with substrates used enzyme at an initial concentration of 0.6 mM. In these experiments, the enzyme (at pH 5 and 8) was preincubated with a 2-fold excess of substrate for 5 min at room temperature, prior to the 2 s reaction (in ice) with an equal volume of a 5-fold excess of H_2O_2 (buffered at the same pH as the enzyme). The EPR spectrum of the native protein was always recorded before and after incubation with the substrate to test possible changes in the ferric spectrum induced by substrate binding close to the heme.

Stopped-Flow UV−Vis Absorption Measurements. The time-dependent absorption spectra were obtained using a four-syringe SX20 stopped-flow spectrophotometer (Applied PhotoPhysics Ltd.) equipped for conventional and sequential stopped-flow measurements with an attached diode array detector. A refrigerating bath (Huber Minichiller) was used to regulate the temperature of the samples in the syringes and in the mixing cell at 5 and 20 °C. All measurements were performed using an optical cell with a path length of 1 cm, and the shortest time for mixing and recording the first data point was 1.26 ms. For the dual-mixing experimentsm LPO samples were at an initial concentration of 0.016 mM and mixed with an equal volume of hydrogen peroxide at 0.08 mM (5-fold excess). Sequential mixing stopped-flow experiments were used to determine the reaction between the preformed [Fe(IV)═O Por$^{\bullet+}$] intermediate and the five different substrates. For these experiments, the enzyme (at 0.032 mM) was mixed with an equal volume containing a 5-fold excess of hydrogen peroxide (at 0.16 mM), and after an aging time of 50 ms, the resulting intermediate was further mixed with an equal volume containing an equimolar substrate (at 0.016 mM), for each of the five substrates. All reagents (enzyme, hydrogen peroxide, and substrates) were in 50 mM Tris-maleate buffer at pH 8.0 or 5.2. Data were recorded using 1000 data points on a logarithmic scale and over a total time of 5 s. Data analysis was done using singular-value decomposition (SVD) with the Pro-K.2000 Global Analysis program (Applied PhotoPhysics Ltd.) to fit the time-dependent spectra and obtain the observed transition rates (k_n) between species.

RESULTS

Characterization of the Radical Intermediates Using Multifrequency EPR Spectroscopy. We have previously shown that the enhanced resolution of the **g** tensor of protein-based radicals obtained with high-field/high-frequency (285 GHz/10 T) EPR spectroscopy is required to distinguish tyrosyl and tryptophanyl radicals contributing to the EPR spectrum of radical intermediates formed in the catalytic

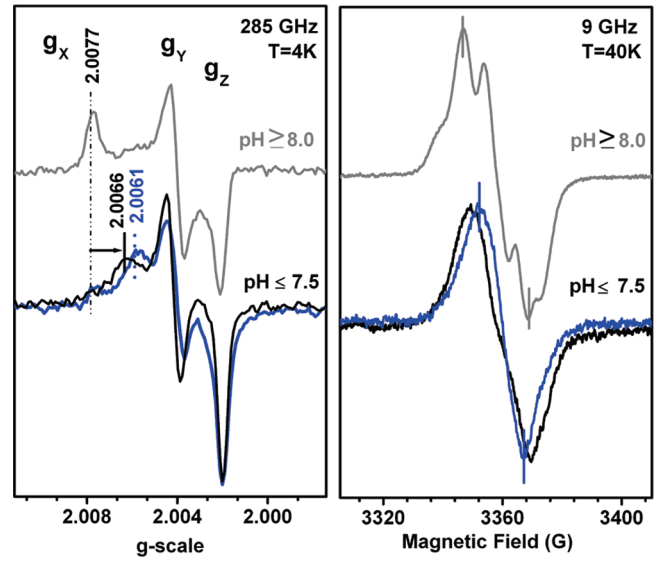

FIGURE 1: EPR spectra at 285 GHz (left) and 9 GHz (right) of the protein-based radicals formed by the reaction of lactoperoxidase with a 5-fold excess of hydrogen peroxide (except for the spectrum in blue trace, 15-fold) at 0 °C and at different pH values. The 9 GHz spectra were recorded at 40 K, with a modulation amplitude of 1 G, a microwave power of 0.08 mW, and a modulation frequency of 100 kHz. The 285 GHz spectra (shown in *g* scale) were recorded at 10 K, using a frequency modulation of 30 kHz and a field modulation of 10 G.

cycle of peroxidases (*21, 33*−*35*). In the case of LPO, formation of two protein-based radicals was previously proposed (*24*), and we therefore investigated these radical species using multifrequency EPR spectroscopy. Figure 1 shows the 285 and 9 GHz EPR spectra of LPO upon reaction with a 5-fold excess of hydrogen peroxide and as a function of pH ($4 \leq pH \leq 10$). For both frequencies, the spectra at pH 8 shown in Figure 1 (top) are representative of all spectra obtained for samples at basic pH values (pH ≥8), and the spectra at pH 5 (bottom) are representative of those obtained at neutral and acidic pH values ($4 \leq pH \leq 7.5$). The 285 GHz EPR spectrum (Figure 1, left) exhibits three main resonances that were consistent with the principal *g* values of tyrosyl radicals formed in enzymes (*36* and references therein) or by γ-irradiation of Tyr crystals (*33*). The spectrum of the pH 8 sample (top, gray trace) could be best simulated with *g* values of 2.0077(0), 2.0039(5), and 2.0020(8) for g_x, g_y, and g_z, respectively. The spectrum at pH 5 (bottom, black trace) exhibited a smaller *g* anisotropy (defined as $\Delta g = |g_x - g_z|$). It could be best simulated with a g_x value of 2.0066(2) and a distribution in g_x with a Gaussian width of 0.0007 to account for the broad g_x component. The *g* anisotropy of the 285 GHz EPR spectrum of LPO at pH 8 was very similar to that of $Tyr_D^{\bullet}$ in photosystem II, and at pH 5, the *g* anisotropy and g_x distribution of the spectrum resembled those of Tyr$^{\bullet}$ in the W191G mutant of cytochrome *c* peroxidase (see Figure 6 of ref *33*). The presence of a well-ordered H-bond of intermediate strength to the radical or a distributed electropositive environment was previously correlated to the specific features of the HF EPR spectra of the PSII and CcP tyrosyl radicals, respectively. In addition, the HF EPR spectrum of the LPO radical formed at pH 5 upon reaction with a greater excess (15-fold) of hydrogen peroxide exhibited a small but measurable shift in the g_x component, with a g_x value of 2.0061(0) (bottom, blue trace). Such a

shift is indicative of a further change in the environment of the tyrosyl radical as a function of pH.

The 9 GHz EPR spectra (Figure 1, right) of the same samples measured at 285 GHz (Figure 1, left) exhibited radical signals with clearly different overall widths and shapes at pH 8 and 5, indicating a pH-dependent difference in the (unresolved) proton hyperfine couplings that dominate the tyrosyl radical spectra at this frequency. The spectrum of the pH 5 enzyme upon reaction with a greater excess (15-fold) of H_2O_2 exhibited a narrower signal (peak-to-trough of 15 G; right panel, blue trace) as compared to the 5-fold excess case (peak to trough of 20 G; right panel, black trace). Taken together, the differences in **g** tensor (g_x values) and proton hyperfine couplings detected in the EPR spectra recorded at 285 and 9 GHz, respectively, agree well with two chemically different Tyr radicals formed as a function of pH. Accordingly, a hydrogen-bonded tyrosine with a pH-dependent strength or two physically different tyrosines with different microenvironments would be consistent with the EPR data. Interestingly, the different microenvironment of Tyr$^{\bullet}$ could be related to the reactivity of the radical (see Discussion), as previously shown in the case of the photosystem II Tyr_D and Tyr_Z radicals (*32* and references therein).

Another feature revealed by the 285 GHz EPR spectrum of LPO upon reaction with hydrogen peroxide was the additional intensity contributing to the $g_y - g_z$ spectral region of the Tyr radical signal. Such a signal exhibited a g anisotropy totally consistent with that expected for a tryptophanyl radical (*36* and references therein). A similar case was reported for *Synechocystis* and *M. tuberculosis* catalase-peroxidases that showed the contribution of a Trp$^{\bullet}$ species and a Tyr$^{\bullet}$ species to their HF EPR spectra (*37, 21*), and for which the changes of the 9 GHz EPR radical spectrum upon selective (Tyr and Trp) deuteration of the samples confirmed the assignment of the less anisotropic HF EPR signal to a Trp radical.

Lactoperoxidase Intermediates Monitored by Stopped-Flow Optical Measurements and EPR Spectroscopy. We have previously shown that the electronic absorption spectrum of an [Fe(IV)═O] intermediate, so-called Compound II, is indistinguishable from that of an [Fe(IV)═O Tyr$^{\bullet}$] or [Fe(IV)═O Trp$^{\bullet}$] species, so the EPR spectrum is required for the assignments (*21, 25*). Accordingly, we have combined the information obtained from the rapid-scan absorption and the EPR spectra on the reactive intermediates to facilitate the analysis of the catalytic intermediates in LPO and their reactivity with substrates. The reaction of LPO with hydrogen peroxide was monitored using conventional dual-syringe mixing and a diode array detector attached to the stopped-flow machine. To combine the information about intermediates obtained from stopped-flow and EPR experiments, all the stopped-flow studies were carried out at 5 °C. The absorption spectral changes observed when measurements were taken at 5 °C (Figure 2) and 22 °C (Figure S1 of the Supporting Information) were qualitatively the same, and only the observed rates differed (Table 1).

Figure 2 shows the changes in the electronic absorption spectrum of LPO at pH 8 (top) and pH 5 (bottom), upon reaction with hydrogen peroxide (5-fold excess) and as a function of time on a millisecond time scale up to 5 s. The native spectrum of LPO (Figure 2, black trace) shows the ferric (high-spin) heme with the characteristic Soret band at 411 nm and the charge transfer (CT) band at 640 nm for both pH 8 and 5. At pH 8 (Figure 2A), a well-defined new species with clear hypochromicity of the Soret band, a shift of the CT band to 660 nm, and a band at 600 nm was observed in 35 ms (Figure 2A, thick green trace). A progressive transition (green traces) leads to the final spectrum, with the Soret band shifted to 433 nm and two distinct new CT bands at 536 and 566 nm (Figure 2A, red traces) and was completed within 2 s (thick red trace). Spectral analysis was used to treat the time-dependent experimental data (see Experimental Procedures). A two-step model (A → B → C) in which A is the ferric enzyme reproduced well the observed spectral changes described above with the following observed rate constants: $k_1 = 550$ s^{-1} and $k_2 = 1$ s^{-1} (Table 1). The absorption spectrum of intermediate B (Figure 2A, thick green trace) agreed well with the well-characterized [Fe(IV)═O Por$^{\bullet+}$] intermediate in horseradish peroxidase, for which the assignment of the chemical nature of the intermediate was supported by the corresponding 2000 G broad EPR spectrum (*38*). The spectrum of the final intermediate, C (Figure 2A, thick red trace), agreed well with the ferryl species, so-called Compound II of horseradish and plant peroxidases (reviewed in ref *3*) but also with the [Fe(IV)═O Tyr$^{\bullet}$] species in bovine liver catalase (*25*). As mentioned previously, EPR parallel measurements are necessary to assign the species (see below). When the reaction of the enzyme with H_2O_2 (5-fold excess) was monitored at pH 5 (Figure 2B), the observed spectral changes and intermediates were very similar to those described for the pH 8 enzyme, although a clearly slower formation of the first intermediate (Figure 2B, thin green traces) and a modestly faster transition to the final spectrum (Figure 2B, thick red trace) were observed. Spectral analysis using a two-step model (A → B → C) to fit the pH 5 experimental data resulted in observed rate constants of 37 s^{-1} for the transition between the Fe(III) enzyme and the [Fe(IV)═O Por$^{\bullet+}$] intermediate as compared to 550 s^{-1} at pH 8 (see Table 1).

Table 1: Calculated Rate Constants (k_{obs}, s^{-1}) for the Reaction of LPO with Hydrogen Peroxide as a Function of Temperature and pH Values Using a Two-Step Model [A → B → C, with k_1 and k_2 (bold)] and a Three-Step Model [A → B → B′ → C with k_1, $k_{1'}$, and k_2 (in parentheses)]

	pH 8				pH 5			
	5 °C		22 °C		5 °C		22 °C	
k_1	**550**	(552)	**1206**	(1192)	**37**	(38)	**139**	(134)
$k_{1'}$		(4)		(6)		(3)		(5)
k_2	**1**	(0.5)	**2**	(1.5)	**1**	(1)	**4**	(2)

It is of note that the 600 nm band (green trace) is an unusual feature for the typical [Fe(IV)═O Por$^{\bullet+}$] absorption spectrum in plant peroxidases. Such a feature was previously detected upon reaction of LPO with H_2O_2 (*18*) and with HOCl (*19*), thus indicating it does not depend on the enzyme preparation or reactant that is used. The 600 nm band was less pronounced in the transitional spectrum observed at 300 ms (Figure 2A, thick blue trace) than in the 35 ms spectrum and was reproduced well (species B′) when using a three-step model (A → B → B′ → C) for spectral fitting (Figure S2A of the Supporting Information). It is of note that the additional species B′ (with $k_{1'} = 4$ s^{-1}) did not result in substantial changes to k_1 and k_2 of the predominant B and C intermediates obtained with the two-step model. Considering

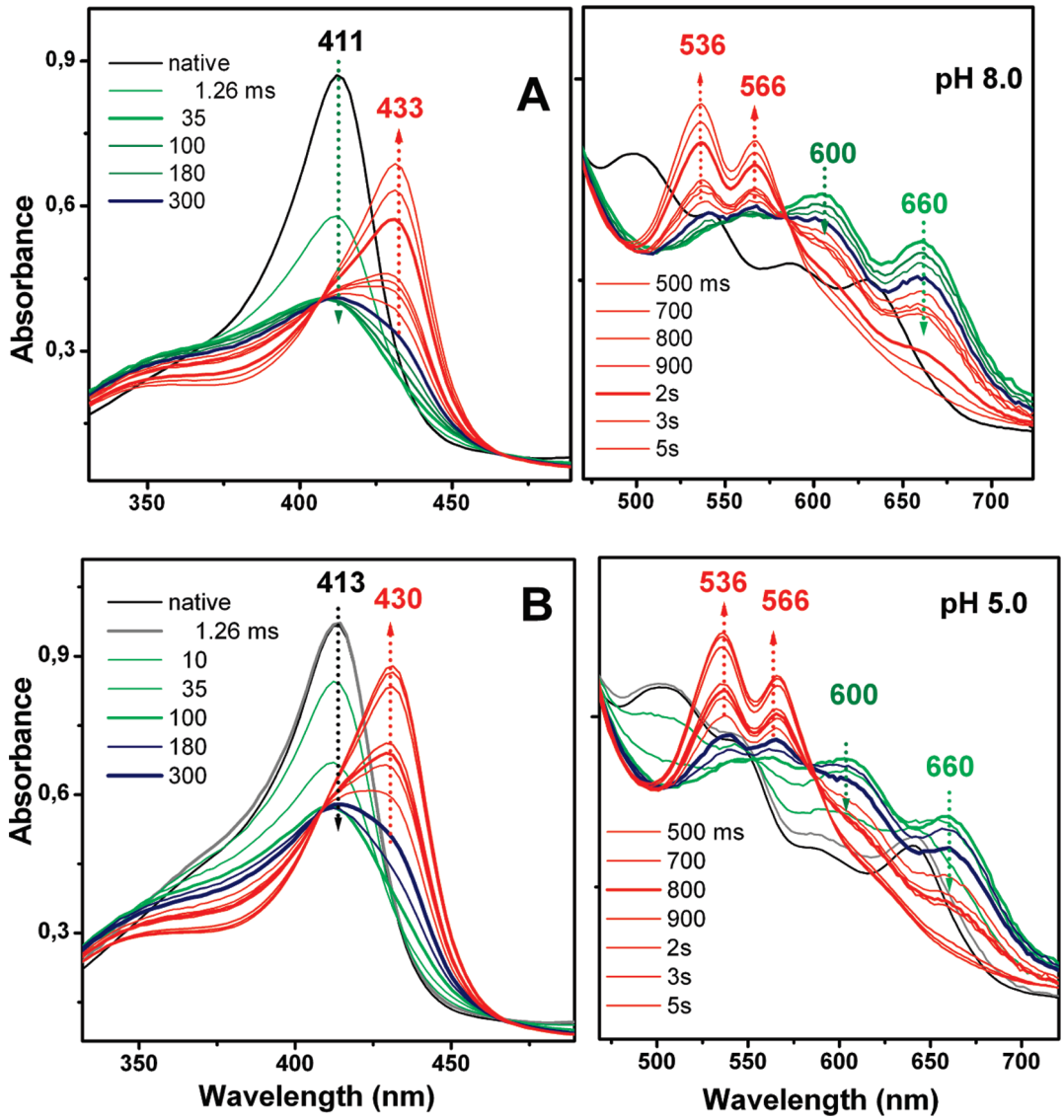

FIGURE 2: Rapid-scan electronic absorption spectrum of the reaction of lactoperoxidase with a 5-fold excess of hydrogen peroxide. The samples and mixing chamber were kept at 5 °C, and the reaction was monitored for up to 5 s. The experiments were conducted at pH 8 (A) and pH 5 (B). Selected representative spectra are shown. The spectrum of the native (ferric) enzyme is colored black, the [Fe(IV)═O Por$^{\bullet+}$] species is green, the ferryl species is red, and the transition [Fe(IV)═O Por$^{\bullet+}$] to [Fe(IV)═O] is blue. The corresponding spectra (species A, B, B′, and C, respectively) fitted to a three-step model are shown in Figure S2 (Supporting Information).

that one of the characteristic bands in the absorption spectrum of Trp radicals (*39*) was detected in the range of 500−600 nm, depending on the protonation state of the radical (*40, 41*), it is tempting to speculate that the contribution of the 600 nm band to the otherwise typical Compound I spectrum of LPO could arise from the equilibrium between the [Fe(IV)═O Por$^{\bullet+}$] species and an [Fe(IV)═O Trp$^{\bullet}$] intermediate. Because of the time scale of the formation of these reactive intermediates, freeze-quench HF EPR spectroscopy may be helpful in possibly detecting a relatively higher contribution of the Trp$^{\bullet}$ signal for shorter mixing times.

As demonstrated by the stopped-flow experiments, the spontaneous decay of the [Fe(IV)═O Por$^{\bullet+}$] intermediate to the species exhibiting characteristics of a ferryl spectrum (see above) in LPO occurs within milliseconds. This behavior differs from that of other peroxidases such as horseradish, ascorbate, and turnip peroxidases in which the [Fe(IV)═O Por$^{\bullet+}$] intermediate is longer-lived. Therefore, the characteristic EPR spectrum of Compound I formed in these enzymes could be detected in samples prepared by manual mixing (*34, 38, 42*). By contrast, the EPR spectrum of the reaction mixture of LPO with hydrogen peroxide (2 s in ice) showed the conversion of the ferric signal and formation of the Trp and Tyr radicals, the oxoferryl species being EPR-silent. It is of note that at pH 8 longer mixing times (15 s) were required to obtain the highest yield of the radical signal as compared to the pH 5 samples (2 s), but in both cases, further mixing in ice showed a decrease in the intensity of the radical signal with no concomitant reappearance of the ferric signal, consistent with the decay to the EPR-silent species favored at pH 5. The stopped-flow experiments confirmed the assignment of the EPR-silent species to the Compound II {[Fe(IV)═O]} intermediate. Moreover, spin quantification (estimated from the double integral of the 40 K EPR radical signal) showed that the yield of Tyr and Trp radicals formed after a mixing time of 2 s of the pH 5 enzyme with a 5-fold excess of H_2O_2 in ice was 40% of that obtained at pH 8.0 (the latter estimated to be 0.4 spin/heme), thus indicating the formation of a higher proportion of the [Fe(IV)═O] intermediate at pH 5.0. These results are

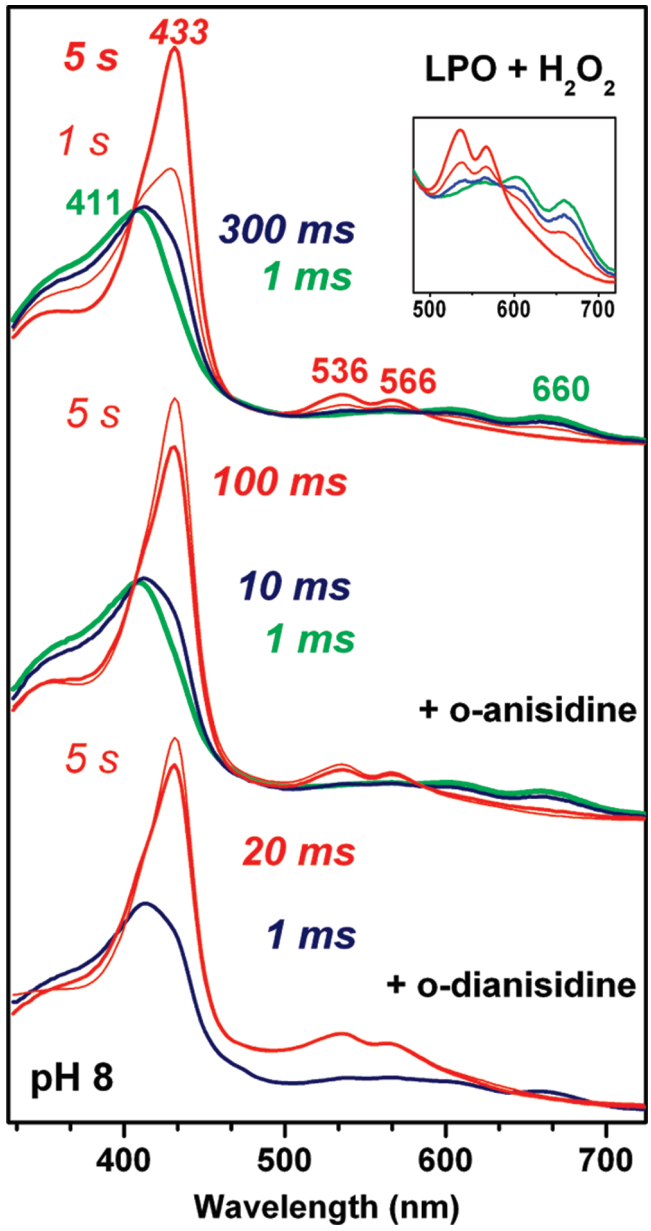

FIGURE 3: Rapid-scan electronic absorption spectra of the reaction of the [Fe(IV)═O $Por^{\bullet+}$] intermediate (pH 8) with *o*-anisidine (middle) and *o*-dianisidine (bottom) as substrates. The control sample (top) corresponds to the use of buffer instead of substrates. Sequential mixing combined with diode array detection was used to monitor the reaction of the preformed [Fe(IV)═O $Por^{\bullet+}$] species with the substrates. The [Fe(IV)═O $Por^{\bullet+}$] intermediate (green trace) was obtained with a 5-fold excess of hydrogen peroxide and a mixing time of 50 ms at 5 °C. Only representative spectra are shown, and in each case, the spectrum labeled 1 ms represents the first spectrum obtained upon reaction of the preformed [Fe(IV)═O $Por^{\bullet+}$] species with substrates (or with buffer for the control). The experimental conditions are further described in Experimental Procedures.

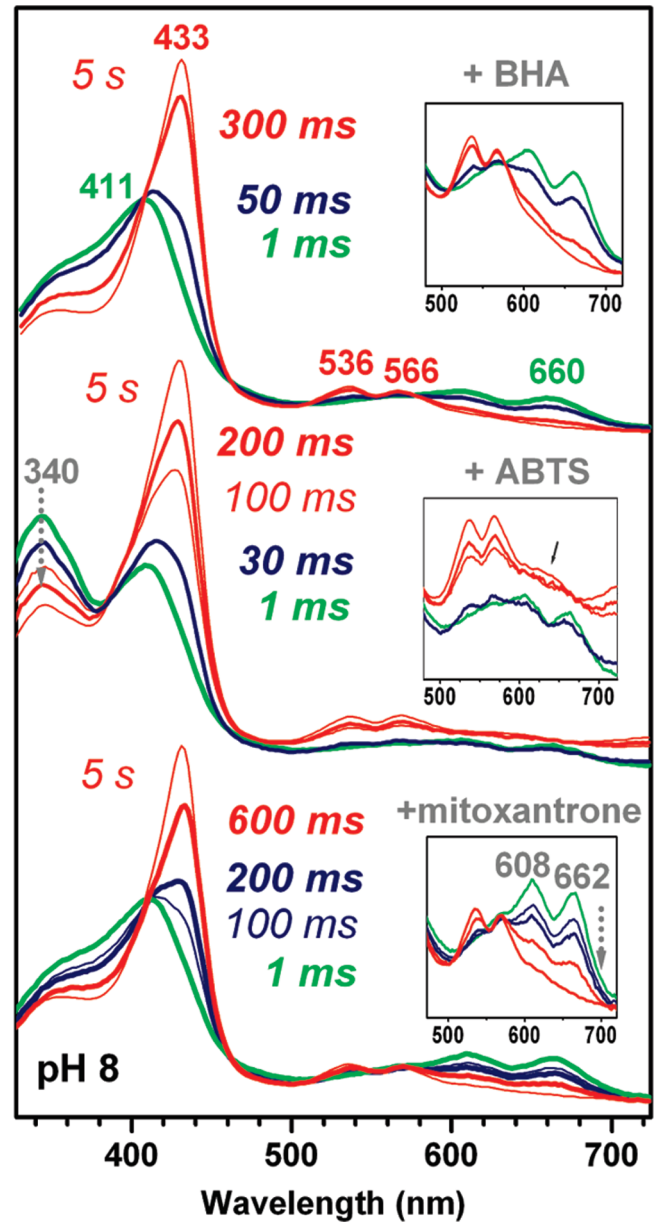

FIGURE 4: Rapid-scan electronic absorption spectra of the [Fe(IV)═O $Por^{\bullet+}$] intermediate (pH 8) reaction with BHA (top), ABTS (middle), and mitoxantrone (bottom). Sequential mixing combined with diode array detection was used to monitor the reaction of the preformed [Fe(IV)═O $Por^{\bullet+}$] intermediate with the substrates. The control experiment (substrate-free reaction) is shown in Figure 3 (top), and the experiments were performed as described in the legend of Figure 3. Experimental conditions are further described in Experimental Procedures.

consistent with a different stability of the radicals as a function of pH, possibly related to the different microenvironment of the Tyr radical predicted from the HF EPR spectra. A similar situation was observed for (dark-stable) $Tyr_D^{\bullet}$ and $Tyr_Z^{\bullet}$ in photosystem II (*32*).

Reaction of Lactoperoxidase with Substrates. We monitored the reaction of five different substrates using the sequential mixing technique in combination with a diode array detector. To preform the [Fe(IV)═O $Por^{\bullet+}$] intermediate, the enzyme at pH 8.0 was mixed with a 5-fold excess of hydrogen peroxide in the aging loop and incubated for 50 ms, prior to the reaction with the different substrates at equimolar concentrations. The control spectrum for these experiments was obtained using buffer instead of substrates (Figure 3, top), and the first recorded spectrum (green trace) is that of the [Fe(IV)═O $Por^{\bullet+}$] intermediate described in the previous section (see Figure 2A, thick green trace).

o-Dianisidine, o-Anisidine, and Benzohydroxamic Acid. *o*-Dianisidine is commonly used as a one-electron donor substrate for peroxidases. The first spectrum recorded 1 ms after the reaction of the preformed [Fe(IV)═O $Por^{\bullet+}$] intermediate with *o*-dianisidine (Figure 3, bottom, blue trace)

Table 2: Specific Peroxidase Activity (SA, micromoles per minute per micromole of heme) of Lactoperoxidase for Different Substrates

	pH 8		pH 5	
	5 °C	22 °C	5 °C	22 °C
o-dianisidine[a]	2118	4651	1108	5649
o-anisidine[b]	276	588	138	339
o-anisidine[c]	260	612	334	671
ABTS[d]	0.5	4	625	6418
ABTS[e]	0.5	5	615	1426

[a] Reaction monitored at 460 nm. [b] Reaction monitored at 450 nm. [c] Reaction monitored at 500 nm. [d] Reaction monitored at 405 nm. [e] The reaction of *M. tuberculosis* catalase-peroxidase, H_2O_2, and ABTS (monitored at 405 nm) is shown for comparison.

was equivalent to that of the transitional spectrum observed at 300 ms of the spontaneous decay of the enzyme (Figure 3, top, blue trace). This result indicated a faster conversion to the [Fe(IV)═O] species due to the one-electron oxidation of *o*-dianisidine by the [Fe(IV)═O Por$^{\bullet+}$] intermediate. A full conversion to the oxoferryl oxidation state (433, 536, and 566 nm bands) was observed 20 ms after the reaction (Figure 3, bottom, red trace), instead of the 5 s required for the spontaneous transition of the enzyme in the absence of substrate (Figure 3, top, thick red trace). The data were fitted to a one-step model {[Fe(IV)═O Por$^{\bullet+}$] → [Fe(IV)═O]} with observed rate constants of 78 s^{-1} for *o*-dianisidine as compared to 1 s^{-1} for the control case (see Table S1). When using *o*-anisidine as a substrate (Figure 3, middle), equivalent spectral changes occurred at longer times than in the case of *o*-dianisidine. The full conversion to the [Fe(IV)═O] species was completed in ~100 ms, indicating a slower reaction with *o*-anisidine. Accordingly, the peroxidase specific activities determined under comparable conditions (pH 8 and 5 °C) revealed that of *o*-anisidine to be one-tenth of that of *o*-dianisidine (Table 2). The reaction (at 5 °C) of the preformed [Fe(IV)═O Por$^{\bullet+}$] intermediate with benzohydroxamic acid showed that the full conversion to the oxoferryl spectrum was obtained within 300 ms (Figure 4, top, thick red trace). The estimated rate constant was 5 s^{-1} (see Table S1), or approximately one-tenth of that of *o*-dianisidine (78 s^{-1}). The parallel EPR experiments showed the conversion of the ferric signal to an EPR-silent species, thus confirming that the bands observed in the absorption spectrum correspond to the [Fe(IV)═O] species.

ABTS and Mitoxantrone. ABTS is another commonly used artificial substrate for peroxidases (see, for example, refs *43* and *44*) despite the larger size of the molecule compared to aromatic substrates. This would possibly mean a different accessibility to the enzyme and binding site for ABTS as compared to that of *o*-dianisidine (or other small substrates). When the preformed [Fe(IV)═O Por$^{\bullet+}$] intermediate was mixed with ABTS at pH 8, the first recorded spectrum (Figure 4, middle, green trace) was identical to the enzyme control spectrum plus the additional band at 340 nm (see the arrow in Figure 4, middle) of the neutral ABTS molecule (*45*). Progressive conversion to the oxoferryl spectrum of the enzyme with the concomitant intensity decrease of the 340 nm band of neutral ABTS started 30 ms after reaction (see the gray arrow in Figure 4, middle). The 200 ms spectrum showed the full conversion to the oxoferryl intermediate (bands at 433, 536, and 566 nm), the disappearance of the ABTS band (340 nm), and the concomitant appearance of the new features that agreed well with the

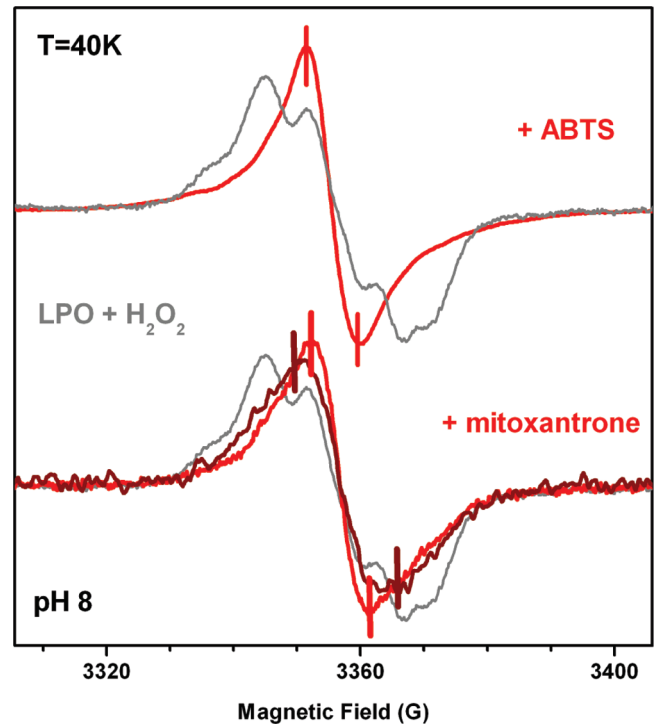

FIGURE 5: EPR spectra at 9 GHz of the radicals formed upon reaction of lactoperoxidase with ABTS (top, red trace) and mitoxantrone (bottom, red trace). The enzyme (pH 8) was preincubated with a 2-fold excess of substrate in the EPR tube, prior to the manual mixing with a 5-fold excess of hydrogen peroxide (4 s reaction time in ice). The spectrum of the control reaction of the enzyme at pH 8 with a 5-fold excess of hydrogen peroxide (gray trace) is also shown. The mitoxantrone radical spectrum obtained with the enzyme at pH 5 is also shown (bottom, dark red trace). The signal intensities of the ABTS and mitoxantrone radicals were scaled down to that of the control (gray trace) for the sake of comparison. Spectra were recorded at 30 K with a modulation amplitude of 2 G, a microwave power of 0.16 mW, and a modulation frequency of 100 kHz.

ABTS radical species (*45*). Specifically, the contribution of the 417 nm band from the ABTS radical to the enzyme Soret band and the rising baseline with a band at 645 nm (Figure 4, middle, inset) were totally consistent with the expected bands at 417, 645, and 728 nm of the ABTS radical (see Figure S3 of the Supporting Information). Clear evidence of these assignments was given by the EPR experiments, in which the enzyme was preincubated with ABTS prior to the reaction with H_2O_2. The EPR spectrum showed the conversion of the ferric signal and the sole radical formed (Figure 5, top, red trace) was consistent with an ABTS radical (*45*). This radical signal was quite distinct from the Tyr$^{\bullet}$ and Trp$^{\bullet}$ species formed in the control experiment (Figure 5, top, gray trace) considering the rather narrow peak-to-trough width (9 G), different relaxation properties, the yield, and the higher stability. Moreover, the concomitant intensity decrease of the ferric EPR signal of the resting enzyme (20% of the native LPO ferric signal) upon reaction with hydrogen peroxide confirmed the formation of the (EPR-silent) oxoferryl species, as detected in stopped-flow experiments and resulting from the one-electron oxidation reaction of the [Fe(IV)═O Por$^{\bullet+}$] intermediate with ABTS. The stopped-flow experiments on the pH 5 enzyme showed the same trend as for pH 8, except for a more efficient oxidation of ABTS, considering that the full conversion of the enzyme to the oxoferryl spectrum and concomitant formation of the ABTS

radical were observed within 100 ms. The EPR experiments showed an almost complete conversion of the ferric enzyme (virtually no ferric signal was detected upon reaction with hydrogen peroxide of the enzyme premixed with ABTS) and a 25% higher yield of the ABTS radical as compared to the pH 8 case. Accordingly, the specific activity of the enzyme was *600 times higher at pH 5 than at pH 8* (Table 2), a behavior that none of the other substrates showed (see Discussion).

A thorough characterization of the reaction of LPO with mitoxantrone by stopped-flow spectrophotometry has been reported previously (*46*) and will not be repeated here. The absorption spectrum of mitoxantrone (*46*), with two predominant bands at 608 and 662 nm (Figure 4, bottom, inset), overlapped with the spectral region of the enzyme between 500 and 750 nm, thus masking the charge transfer band at 660 nm of the [Fe(IV)═O Por$^{\bullet+}$] intermediate (see Figure 3, top, inset). However, the reaction of the enzyme with equimolar mitoxantrone could be monitored by the changes of the heme Soret band for the enzyme and the concomitant decrease in the magnitude of the mitoxantrone bands at 608 and 662 nm (Figure 4, bottom). The radical product of mitoxantrone was previously reported to have a broad band centered at 750 nm (*46*), thus outside the detection range of our spectrophotometer, but formation of the radical could be monitored by our parallel EPR experiments (see below). Under our experimental conditions, the first spectrum recorded after the reaction of the preformed [Fe(IV)═O Por$^{\bullet+}$] intermediate (enzyme at pH 8) with mitoxantrone showed the same enzyme spectrum as in the control reaction with the additional mitoxantrone bands at 608 and 662 nm (Figure 4, bottom). The 200 ms spectrum showed the formation of an oxoferryl-like intermediate of the enzyme, and the bleaching of the mitoxantrone bands (see the arrow in Figure 4, bottom, inset). A complete bleaching of the mitoxantrone bands and the concomitant full formation of an oxoferryl spectrum (433, 536, and 566 nm) were observed at 600 ms (see Figure 4, bottom, thick red trace). The EPR experiments showed that when LPO was incubated with mitoxantrone prior to the reaction with hydrogen peroxide, a narrow radical signal (peak to trough of 9 G; Figure 5, bottom, red trace) rather different from that of the control experiment (gray trace) was detected. This radical agreed well with the signal previously reported for the reaction of HRP with mitoxantrone (*47*). When using the enzyme at pH 5, a broader radical signal (peak to trough of 15 G) was formed in lower yield (Figure 5, bottom, dark red trace) and the stopped-flow experiments showed a slower reaction of the [Fe(IV)═O Por$^{\bullet+}$] species with mitoxantrone at pH 5. The broader EPR spectrum at pH 5 indicates the contribution of the Tyr$^{\bullet}$ and mitoxantrone radical signals. Taken together, these results suggest a possible competition between the oxidation of mitoxantrone and the formation of the [Fe(IV)═O Tyr$^{\bullet}$] species at pH 5.

DISCUSSION

The formation of a putative protein-based radical intermediate isoelectronic to the [Fe(IV)═O Por$^{\bullet+}$] species in the catalytic cycle of lactoperoxidase has been previously suggested by a number of studies (reviewed in ref *23*), yet the sole experimental evidence to date of the formation of a protein-based radical upon reaction of the enzyme with hydrogen peroxide was obtained with spin trapping experiments (*24*). In the work presented here, we have used multifrequency EPR spectroscopy to directly detect the radical(s) and determine their electronic nature and microenvironment as well as the putative catalytic competence of such radicals. As described in Results, the 285 GHz EPR spectrum obtained upon reaction of LPO with hydrogen peroxide unequivocally showed the predominant signal of a tyrosyl radical. It has been demonstrated previously by HF EPR experiments and semiempirical calculations that the **g** tensor component in the direction of the phenoxyl C−O bond (defined as the g_x component) reflects differences in the electrostatic microenvironment of tyrosyl radicals (*36* and references therein) that can be resolved by using the advantageous resolution of the g anisotropy (defined as $|g_x - g_z|$) in protein-based radicals when measuring at higher fields (higher frequencies). The experimentally observed g_x values, confirmed by the theoretical predictions, range between 2.0089(6) in the case of nonpolar environments as for *Escherichia coli* ribonucleotide reductase (RNR) Tyr$^{\bullet}$ (*48*) and 2.0066(0) in the case of a strong H-bond as for the in vitro Tyr$^{\bullet}$ radical generated in crystals of Tyr-HCl (*31*). Accordingly, the g_x values of the lactoperoxidase Tyr$^{\bullet}$ [2.0077(0) at pH ≥8 and 2.0066(2) at pH ≤7.5 (Figure 1)] indicate an electropositive environment for the radical, implying a hydrogen bond interaction and/or the presence of a nearby positively charged residue (*49*). Screening the crystal structure of the enzyme for tyrosine residues having such an environment is an effective approach to identify possible candidates for the radical site, since all tyrosines with an environment that is not in agreement with that predicted by the HF EPR spectrum can be confidently ruled out. This approach is particularly useful for proteins with a large number of tyrosines (15 in lactoperoxidase). Accordingly, inspection of the crystal structure of LPO (PDB entry 2GJ1) indicates that two-thirds of the tyrosines can be ruled out as radical sites: (i) Tyr37, Tyr118, Tyr156, Tyr313, and Tyr350 because they lack potential H-bond partners or positively charged amino acids at distances shorter than 9 Å and (ii) Tyr210, Tyr277, Tyr296, Tyr316, and Tyr557 (all within H-bonding distance of a structural water molecule) because a global pH-induced structural change of the enzyme after reaction with hydrogen peroxide would have to occur to reflect the pH-dependent change in the Tyr$^{\bullet}$ environment predicted by the HF EPR spectra.

Table 3: Microenvironment of the Putative Candidates for the Tyrosyl Radical Site in Lactoperoxidase (PDB entry 2GJ1; structure at pH 8.0)

	Tyr7	Tyr71	Tyr433	Tyr468	Tyr177
H-bond partner	Glu279	Glu74	Glu483	Asp475	His257
H-bond distance (Å)	1.44	1.50	1.46	1.7	1.87
Lys or Arg residue	Lys275	Lys390	Arg437	Arg426	−
N_{Lys}−O_{Tyr} distance (Å)	3.0	4.5	3.9	4.2	−
O_{Tyr}−Fe distance (Å)	33.7	15.3	21.8	18.1	23.2

Therefore, only five tyrosines are good candidates for the radical site because they all have polar microenvironments that are consistent with the expected pH-dependent behavior predicted by the HF EPR spectra. Specifically, Tyr7, Tyr71, Tyr433, and Tyr468 have the carboxylate of a glutamic (or aspartic) acid as the proton acceptor in a strong H-bond and a nearby (positively charged) lysine (or arginine). Thus, the

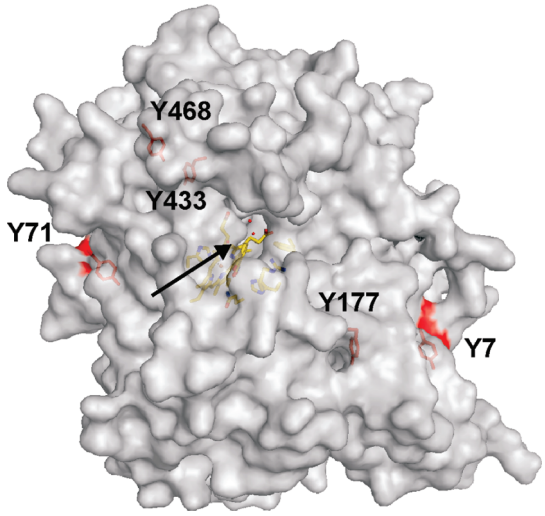

FIGURE 6: Global view of the structure of lactoperoxidase highlighting the five tyrosine residues (see Table 3) which are the only candidates for the radical site based on the high-field EPR spectroscopy studies in this work. The black arrow indicates the access channel, with the heme partially visible at the end of it. This figure was prepared using the coordinates deposited in the Protein Data Bank (entry 2GJ1).

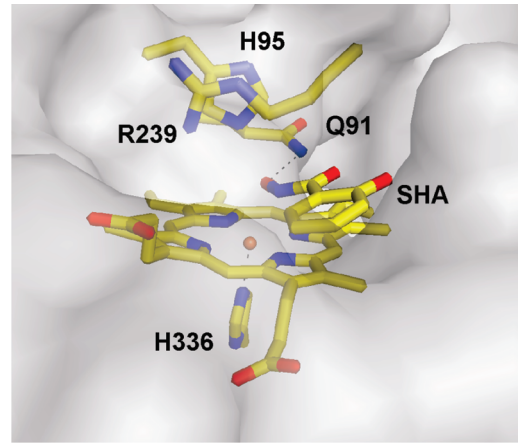

FIGURE 7: Heme active site of lactoperoxidase with 2-hydroxybenzohydroxamic acid (SHA) bound on the distal side. This figure was prepared using the coordinates deposited in the Protein Data Bank (entry 2QPK). SHA binds in the proximity of the distal His and the pentacoordinated heme iron (no direct coordination to the iron). The side view to the access channel allows the substrate to be seen at the end of the access channel. For easier comparison, the numbering used for the labeled amino acids corresponds to that of the substrate-free structure (entry 2GJ1) (see the explanation about the numbering in footnote 2).

observed low g_x value at acidic/neutral pHs is consistent with the (strong) H-bond formed by the carboxyl group of Glu (or Asp), and the distribution of $g_x$values would reflect the influence of the positively charged nearby Lys (or Arg) within 3−4.5 Å, the latter persisting as a weaker interaction at basic pH. Tyr177, for which a histidine residue (His257) is within H-bonding distance through the N_δ position (the N_ε atom being H-bonded to the carbonyl group of Gly195), is also a suitable candidate for the radical site. In this case, the H-bond interaction would be stronger at pH ≤7.5. A comparable situation was previously reported in the case of photosystem II $Tyr_D^\bullet$ (*50*), where the HF EPR spectrum also showed a clear difference in the g_x value for the radical generated by illumination at 1.8 K [g_x value of 2.0064(3)] as compared to that generated at room temperature [g_x value of 2.0075(6)]. It should be noted that we cannot rule out the possibility of two physically different tyrosines being the radical sites, provided they fulfill the requirement of having different (pH-dependent) microenvironments. In such a case, a combination of Tyr177 and one of the four other candidates would be consistent with the HF EPR spectra.

In conclusion, this study allowed us to restrict the possible candidates for the radical site to five well-defined tyrosines (Figure 7): Tyr433 and Tyr468 are close to the surface, Tyr7 and Tyr71 are directly exposed to it, and Tyr177 is located deeper in the protein adjacent to a putative secondary access channel for substrates. A relevant aspect is the fact that the clear change in the electropositive microenvironment (most possibly H-bonding strength) of the tyrosyl radical at neutral and acidic pHs appears to be correlated to the higher reactivity of this species (see below). The surface Tyr156[2] previously identified as the site of dityrosine formation and consequent enzyme dimerization, upon reaction of the enzyme with hydrogen peroxide (*24*), has an environment which is inconsistent with that predicted by the $Tyr^\bullet$ HF EPR spectrum. Also, the previously proposed role of a tyrosyl radical in the oxidation of para-substituted phenols (*6*) may require revision considering that the binding site for aromatic substrates is very close to the heme (as revealed by the crystal structures) and our findings with respect to the relatively long distance from the Tyr radical site to the heme (Table 3).

Mechanisms of Substrate Oxidation. Previous reports of very detailed kinetic studies on the intermediates of LPO and their reaction with substrates using stopped-flow spectrophotometry were all performed at room temperature (*6, 18, 19, 46*). In our work, we have demonstrated the advantage of monitoring the reactions using a combination of EPR and stopped-flow measurements, both at low temperatures, to discriminate between the protein-based radical intermediates and [Fe(IV)═O], to detect the oxidation products of the substrates, and to resolve more clearly the substrate oxidation reactions, which at room temperature happen within the dead time of the stopped-flow instrument [as in the case of thiocyanate (*19*)]. Accordingly, our experiments showed that upon reaction of LPO with hydrogen peroxide at 5 °C, a short-lived [Fe(IV)═O $Por^{\bullet+}$] intermediate is formed within 35 ms at pH 8 and within 100 ms at pH 5 with subsequent fast transitions to [Fe(IV)═O $Tyr^\bullet$] and [Fe(IV)═O] species. To address the question of whether the protein radicals play a role either in direct substrate oxidation or in the electron transfer pathway between the heme and certain substrates, we characterized the reaction of the [Fe(IV)═O $Por^{\bullet+}$] intermediate with five different substrates as a function of temperature and pH. Three of the substrates, benzohydroxamic acid, *o*-dianisidine, and *o*-anisidine, were expected to bind very close to the heme on the basis of the crystal structure of the enzyme, where 2-hydroxybenzohydroxamic

[2] Lardinois and co-workers (*24*) adopted the same numbering as in the model by De Gioia and co-workers (*17*), which referred to the total sequence: 712 amino acids = 100 propeptide residues + 612 amino acids = mature protein. The protein sequences associated with PDB entries 2GJ1 and 2QKT are different from that of the model because the structures are not complete (some fractions of the N-terminus seem to be lacking, and the propeptide is missing). Moreover, the residues in the structures are also shifted as compared to the associated sequence. Thus, Tyr289 in ref *23* corresponds to Tyr156 in 2GJ1 (or Tyr158 in the sequence associated with the structure).

acid is found on the heme-distal side with the aromatic ring lying parallel to the heme plane but not directly coordinated to the heme iron (Figure 7). The substrate-bound structures of the enzyme with thiocyanate and acetylsalicylic acid (PDB entries 2IPS and 2QQT, respectively) showed similar interactions of these substrates with the distal His and heme iron. Accordingly, a heme-edge reaction typical of peroxidases (reviewed in ref *3*) using the [Fe(IV)═O Por$^{\bullet+}$] intermediate is the expected mechanism for the oxidation of these substrates. The observed very fast conversion (within the dead time of the stopped-flow instrument) of the preformed [Fe(IV)═O Por$^{\bullet+}$] intermediate to [Fe(IV)═O] upon reaction with *o*-dianisidine was consistent with such a mechanism. The apparently slower reaction with the benzohydroxamic acid and *o*-anisidine (see Figures 3 and 4 and Table S1) should then arise from the structure of these molecules having different electron donating abilities. Specifically, the larger conjugated double bond or aromatic structure in *o*-dianisidine would favor electron donation as compared to the monophenyl structure of *o*-anisidine and benzohydroxamic acid.

Both mitoxantrone and ABTS are larger molecules and, as such, are not expected to reach the binding site (Figure 7) through the restrictive access channel revealed by the enzyme structure. Accordingly, the oxidation should happen via a long-range electron transfer reaction, the question being whether the oxidizing species is the [Fe(IV)═O Por$^{\bullet+}$] or the tyrosyl radical intermediate. The reaction of LPO with mitoxantrone showed a behavior (similar pH dependency although slower transition to the ferryl species; see Figure 4) comparable with that of benzohydroxamic acid, thus consistent with the [Fe(IV)═O Por$^{\bullet+}$] intermediate being the oxidizing species as previously proposed (*46*). Moreover, our EPR results showing the formation of only the mitoxantrone radical at pH 8 and the contribution of a broader signal, with a peak-to-trough width consistent with the Tyr$^{\bullet}$ signal, at pH 5 strongly indicate that the Tyr$^{\bullet}$ radical is not involved in mitoxantrone oxidation. These findings can be rationalized in terms of a competition between the long-range electron transfer process (favored at pH 8) related to the oxidation of mitoxantrone by the [Fe(IV)═O Por$^{\bullet+}$] intermediate and the intramolecular electron transfer (favored at pH 5) involved in the formation of the [Fe(IV)═O Tyr$^{\bullet}$] species. In the case of ABTS, a unique pH behavior was observed compared to that with other substrates. (a) At pH 5, the ABTS-dependent specific activity was comparable to that of *o*-dianisidine, but it drastically decreased (by 3 orders of magnitude) at pH 8 (Table 1). (b) ABTS was the sole substrate to show an increase in its observed rate constant for the conversion of the preformed [Fe(IV)═O Por$^{\bullet+}$] species to the [Fe(IV)═O] species at pH 5.0 (see Table S1). (c) The yield of ABTS radical was 25% higher at pH 5.0 than at pH 8.0 (inverse behavior for mitoxantrone). Taken together, these results strongly suggest different mechanisms for the oxidation of ABTS and mitoxantrone, possibly related to different binding sites. The efficient reaction of the enzyme with ABTS at pH 5 can be rationalized in terms of the [Fe(IV)═O Tyr$^{\bullet}$] intermediate being the oxidizing species. Interestingly, the peroxidase specific activity of *M. tuberculosis* catalase-peroxidase with ABTS was very similar to that of lactoperoxidase, not only in value but also in the particular pH dependence (see Table 2). We have shown that the [Fe(IV)═O Trp$^{\bullet}$] species {and not the [Fe(IV)═O Por$^{\bullet+}$]} is the reactive intermediate with isoniazid in the *M. tuberculosis* enzyme (*21*).

In conclusion, our studies combining stopped-flow spectrophotometry and EPR spectroscopy have allowed us to carry out a better characterization of the substrate oxidation mechanism involving long-range electron transfer to large substrates that cannot access the binding site close to the heme site in lactoperoxidase. An original aspect of our work as compared to previous studies is the direct detection and characterization of the microenvironment of the tyrosyl radical by multifrequency EPR spectroscopy, which in combination with the recently published crystal structure of the enzyme led to the identification of five specific candidates for the radical site (Figure 6). The well-defined (polar) microenvironment of the tyrosyl radical and its pH dependency support the concept of a discrete location of the radical. Our results are consistent with a pH-dependent competition between substrate oxidation by the [Fe(IV)═O Por$^{\bullet+}$] intermediate (through a long-range electron transfer), illustrated by the case of mitoxantrone, and the formation of the [Fe(IV)═O Tyr$^{\bullet}$] intermediate, the latter being the oxidizing species for ABTS. Lactoperoxidase has been shown to react with a number of organic molecules of relevant pharmacological and toxicological interest, although their structural heterogeneity implies the existence of multiple binding sites. The recently published crystal structures of the enzyme−ligand complexes have identified the binding site for small substrates close to the heme (Figure 7) for which a heme-edge oxidation is expected. The work presented here has resolved two different long-range electron transfer mechanisms, one involving the tyrosyl radical, for the reaction with bulkier substrates. Further use of X-ray crystallography for the identification of the binding site remote from the heme, and related to the more efficient substrate oxidation via the tyrosyl radical, may be a valuable tool in the quest for rational drug design.

ACKNOWLEDGMENT

We thank Sun Un (iBiTec-S, Saclay, France) and Andrew T. Smith (University of Sussex, Brighton, U.K.) for fruitful and stimulating discussions.

SUPPORTING INFORMATION AVAILABLE

Rapid-scan data for the reaction of lactoperoxidase with a 5-fold excess of hydrogen peroxide at 22 °C (Figure S1), SDV analysis of the rapid-scan electronic absorption data at 5 and 22 °C corresponding to the observed transition rates shown in Table 1 (Figure S2), electronic absorption and EPR spectra of the ABTS radical generated by enzymatic reaction and using a low concentration of *M. tuberculosis* catalase-peroxidase (Figure S3), and calculated transition rates for the reaction of the preformed [Fe(IV)═O Por$^{\bullet+}$] intermediate with five different substrates (Table S1). This material is available free of charge via the Internet at http://pubs.acs.org.

REFERENCES

1. Cals, M. M., Guillomot, M., and Martin, P. (1994) The gene encoding lactoperoxidase is expressed in epithelial cells of the goat lactating mammary gland. *Cell. Mol. Biol. 40*, 1143–1150.
2. Wolfson, L. M., and Sumner, S. S. (1993) Antibacterial activity of the lactoperoxidase system: A review. *J. Food Prot. 56*, 887–892.

3. Dunford, B. H. (1999) Lactoperoxidase, thyroid peroxidase, and other animal peroxidases. In *Heme Peroxidases*, pp 414−423, Wiley-VCH, New York.
4. Kussendrager, K. D., and van Hooijdonk, A. C. M. (2000) Lactoperoxidase: Physico-chemical properties, occurrence, mechanism of action and applications. *Br. J. Nutr. 84*, 19–25.
5. Zhang, H., and Dunford, H. B. (1993) Hammet correlation of lactoperoxidase compound II with phenols. *Can. J. Chem. 71*, 1990–1994.
6. Monzani, E., Gatti, A. L., Profumo, A., Casella, L., and Gullotti, M. (1997) Oxidation of phenolic compounds by lactoperoxidase. Evidence for the presence of a low-potential compound II during catalytic turnover. *Biochemistry 36*, 1918–1926.
7. Ferrari, R. P., Laurenti, E., Casella, L., and Poli, S. (1993) Oxidation of catechols and catecholamines by horseradish-peroxidase and lactoperoxidase: ESR spin stabilization approach combined with optical methods. *Spectrochim. Acta, Part A 49*, 1261–1267.
8. Ferrari, R. P., Traversa, S., De Gioia, L., Fantucci, P., Suriano, G., and Ghibaudi, E. M. (1999) Catechol(amine)s as probes of lactoperoxidase catalytic site structure: Spectroscopic and modeling studies. *J. Biol. Inorg. Chem. 4*, 12–20.
9. Metodiewa, D., Reszka, K., and Dunford, H. B. (1989) Oxidation of the substituted catechols dihydroxyphenylalanine methyl ester and trihydroxyphenylalanine by lactoperoxidase and its compounds. *Arch. Biochem. Biophys. 274*, 601–608.
10. Doerge, D. R., and Decker, C. J. (1994) Inhibition of peroxidase-catalyzed reactions by arylamines: Mechanism for the anti-thyroid action of sulfamethazine. *Chem. Res. Toxicol. 7*, 164–169.
11. Josephy, P. D. (1996) The role of peroxidase-catalyzed activation of aromatic amines in breast cancer. *Mutagenesis 11*, 3–7.
12. Gorlewska-Roberts, K. M., Teitel, C. H., Lay, J. O., Roberts, D. W., and Kadlubar, F. F. (2004) Lactoperoxidase-catalyzed activation of carcinogenic aromatic and heterocyclic amines. *Chem. Res. Toxicol. 17*, 1659–1666.
13. Cavalieri, E. L., Stack, D. E., Devanesan, P. D., Todorovic, R., Dwivedy, I., Higginbotham, S., Johansson, S. L., Patil, K. D., Gross, M. L., Gooden, J. K., Ramanathan, R., Cerny, R. L., and Rogan, E. G. (1997) Molecular origin of cancer: Catechol estrogen-3,4-quinones as endogenous tumor initiators. *Proc. Natl. Acad. Sci. U.S.A. 94*, 10937–10942.
14. Sipe, H. J., Jr., Jordan, S. J., Hanna, P. M., and Mason, R. P. (1994) The metabolism of 17β-estradiol by lactoperoxidase: A possible source of oxidative stress in breast cancer. *Carcinogenesis 15*, 2637–2643.
15. Ghibaudi, E. M., Laurenti, E., Beltramo, P., and Ferrari, R. P. (2000) Can estrogenic radicals, generated by lactoperoxidase, be involved in the molecular mechanism of breast carcinogenesis? *Redox Rep. 5*, 229–235.
16. RamaKrishna, N. V., Li, K. M., Rogan, E. G., Cavalieri, E. L., George, M., Cerny, R. L., and Gross, M. L. (1993) Adducts of 6-methylbenzo[α]pyrene and 6-fluorobenzo[α]pyrene formed by electrochemical oxidation in the presence of deoxyribonucleosides. *Chem. Res. Toxicol. 6*, 837–845.
17. De Gioia, L., Ghibaudi, E. M., Laurenti, E., Salmona, M., and Ferrari, R. P. (1996) A theoretical three-dimensional model for lactoperoxidase and eosinophil peroxidase, built on the scaffold of the myeloperoxidase X-ray structure. *J. Biol. Inorg. Chem. 1*, 476–485.
18. Kimura, S., and Yamazaki, I. (1979) Comparisons between hog intestinal peroxidase and bovine lactoperoxidase: Compound I formation and inhibition by benzhydroxamic acid. *Arch. Biochem. Biophys. 198*, 580–588.
19. Furtmüller, P. G., Jantschko, W., Regelsberger, G., Jakopitsch, C., Arnhold, J., and Obinger, C. (2002) Reaction of lactoperoxidase compound I with halides and thiocyanate. *Biochemistry 41*, 11895–11900.
20. Doyle, W. A., Blodig, W., Veitch, N. C., Piontek, K., and Smith, A. T. (1998) Two substrate interaction sites in lignin peroxidase revealed by site-directed mutagenesis. *Biochemistry 37*, 15097–15105.
21. Singh, R., Switala, J., Loewen, P. C., and Ivancich, A. (2007) Two [Fe(IV)═O Trp•] intermediates in *M. tuberculosis* catalase-peroxidase discriminated by multifrequency (9−285 GHz) EPR spectroscopy: Reactivity toward isoniazid. *J. Am. Chem. Soc. 129*, 15954–15963.
22. Seyedsayamdost, M. R., Yee, C. S., Reece, S. Y., Nocera, D. G., and Stubbe, J. (2006) pH rate profiles of F_nY_{356}-R2s ($n = 2$, 3, 4) in *Escherichia coli* ribonucleotide reductase: Evidence that Y_{356} is a redox-active amino acid along the radical propagation pathway. *J. Am. Chem. Soc. 128*, 1562–1568.
23. Ghibaudi, E., and Laurenti, E. (2003) Unraveling the catalytic mechanism of lactoperoxidase and myeloperoxidase. *Eur. J. Biochem. 270*, 4403–4412.
24. Lardinois, O. M., Medzihradszky, K. F., and Ortiz de Montellano, P. R. (1999) Spin trapping and protein cross-linking of the lactoperoxidase protein radical. *J. Biol. Chem. 274*, 35441–35448.
25. Ivancich, A., Jouve, H. M., Sartot, B., and Gaillard, J. (1997) EPR investigation of compound I in *Proteus mirabilis* and bovine liver catalases: Formation of porphyrin and tyrosyl radical intermediates. *Biochemistry 36*, 9356–9364.
26. Stiborová, M., Miksanová, M., Havlícek, V., Schmeiser, H. H., and Frei, E. (2002) Mechanism of peroxidase-mediated oxidation of carcinogenic o-anisidine and its binding to DNA. *Mutat. Res. 500*, 49–66.
27. van der Graaf, W. T., and de Vries, E. G. (1990) Mitoxantrone: Bluebeard for malignancies. *Anti-Cancer Drugs 1*, 109–125.
28. Blanz, J., Mewes, K., Ehninger, G., Proksch, B., Waidelich, D., Greger, B., and Zeller, K. P. (1991) Evidence for oxidative activation of mitoxantrone in human, pig, and rat. *Drug Metab. Dispos. 19*, 871–880.
29. Ferrari, R. P., Laurenti, E., Cecchini, P. I., Gambino, O., and Sondergaard, I. (1995) Spectroscopic investigations on the highly purified lactoperoxidase Fe(III)-heme catalytic site. *J. Inorg. Biochem. 58*, 109–127.
30. Nelson, D. P., and Kiesow, L. A. (1972) Enthalpy of decomposition of hydrogen peroxide by catalase at 25 °C (with molar extinction coefficients of H_2O_2 solutions in the UV. *Anal. Biochem. 49*, 474–478.
31. Lukat, G. S., Rodgers, K. R., and Goff, H. M. (1987) Electron paramagentic resonance spectroscopy of lactoperoxidase complexes: Clarification of hyperfine splitting for the NO adduct of lactoperoxidase. *Biochemistry 26*, 6927–6932.
32. Un, S., Dorlet, P., and Rutherford, A. W. (2001) A high-field EPR tour of radicals in photosystems I and II. *Appl. Magn. Reson. 21*, 341–361.
33. Ivancich, A., Dorlet, P., Goodin, D. B., and Un, S. (2001) Multifrequency high-field EPR study of the tryptophanyl and tyrosyl radical intermediates in wild-type and the W191G mutant of cytochrome c peroxidase. *J. Am. Chem. Soc. 123*, 5050–5058.
34. Ivancich, A., Mazza, G., and Desbois, A. (2001) Comparative electron paramagnetic resonance study of radical intermediates in turnip peroxidase isozymes. *Biochemistry 40*, 6860–6866.
35. Jakopitsch, C., Obinger, C., Un, S., and Ivancich, A. (2006) Identification of Trp106 as the tryptophanyl radical intermediate in *Synechocystis* PCC6803 catalase-peroxidase by multifrequency electron paramagnetic resonance spectroscopy. *J. Inorg. Biochem. 100*, 1091–1099.
36. Un, S. (2005) The g-values and hyperfine coupling of amino acid radicals in proteins: Comparison of experimental measurements with *ab initio* calculations. *Magn. Reson. Chem. 43*, S229−S236.
37. Ivancich, A., Jakopitsch, C., Auer, M., Un, S., and Obinger, C. (2003) Protein-based radicals in the catalase-peroxidase of *Synechocystis* PCC6803: A multifrequency EPR investigation of wild-type and variants on the environment of the heme active site. *J. Am. Chem. Soc. 125*, 14093–14102.
38. Schulz, C. E., Devaney, P. W., Winkler, H., Debrunner, P. G., Doan, N., Chiang, R., Rutter, R., and Hager, L. P. (1979) Horseradish peroxidase compound I: Evidence for spin coupling between the heme iron and a 'free' radical. *FEBS Lett. 103*, 102–105.
39. Solar, S., Getoff, N., Surdhar, P. S., Armstrong, D. A., and Sing, A. (1991) Oxidation of tryptophan and N-methylindole by N_3, Br_2^-, and $(SCN)_2^-$ radicals in light- and heavy-water solutions: A pulse radiolysis study. *J. Phys. Chem. 95*, 3639–3643.
40. Baldwin, J., Krebs, C., Ley, B. A., Edmondson, D. E., Huynh, B. H., and Bollinger, M. (2000) Mechanism of rapid electron transfer during oxygen activation in the R2 subunit of *Escherichia coli* ribonucleotide reductase. Evidence for a transient tryptophanyl radical. *J. Am. Chem. Soc. 122*, 12195–12206.
41. Miller, J. E., Gradinau, C., Crane, B. R., Di Biblio, A. J., Wehbi, W. A., Un, S., Winkler, J. R., and Gray, H. B. (2003) Spectroscopy and reactivity of a photogenerated tryptophan radical in a structurally defined protein environment. *J. Am. Chem. Soc. 125*, 14220–14221.
42. Patterson, W. R., Poulos, T. L., and Goodin, D. B. (1995) Identification of a porphyrin π-cation radical in ascorbate peroxidase compound I. *Biochemistry 34*, 4342–4345.

43. Abelskov, K. A., Smith, A., Rasmussen, C. B., Dunford, H. B., and Welinder, K. G. (1997) pH dependence and structural interpretation of the reactions of *Coprinus cinereus* peroxidase with hydrogen peroxide, ferulic acid, and 2,2′-azinobis(3-ethylbenzthiazoline-6-sulfonic acid). *Biochemistry 36*, 9453–9463.
44. Rodriguez-Lopez, J. N., Gilabert, M. A., Tudela, J., Thorneley, R. N. F., and Garcia-Canovas, F. (2000) Reactivity of horseradish peroxidase compound II towards substrates: Kinetic evidence for a two-step mechanism. *Biochemistry 39*, 13201–13209.
45. Scott, S. L., Chen, W. J., Bakac, A., and Espenson, J. H. (1993) Spectroscopic parameters electrode potentials, acid ionization constants, and electron exchange rates of the 2,2′-azinobis(3-ethylbenzothiazolone-6-sulfonate) radicals and ions. *J. Phys. Chem. 97*, 6710–6714.
46. Bruck, T. B., and Harvey, P. J. (2003) Oxidation of mitoxantrone by lactoperoxidase. *Biochim. Biophys. Acta 1649*, 154–163.
47. Reszka, K. J., Kolodziejczyk, P., and Lown, J. W. (1986) Horseradish peroxidase-catalyzed oxidation of mitoxantrone: Spectrophotometric and electron paramagnetic resonance studies. *J. Free Radical Biol. Med. 2*, 25–32.
48. Un, S., Atta, M., Fontecave, M., and Rutherford, A. W. (1995) g-values as a probe of the local protein environment: High-field EPR of tyrosyl radicals in ribonucleotide reductase and photosystem-II. *J. Am. Chem. Soc. 117*, 10713–10719.
49. Un, S., Gerez, C., Elleingand, E., and Fontecave, M. (2001) Sensitivity of tyrosyl radical g-values to changes in protein structure: A high-field EPR study of mutants of ribonucleotide reductase. *J. Am. Chem. Soc. 123*, 3048–3054.
50. Faller, P., Goussias, C., Rutherford, A. W., and Un, S. (2003) Resolving intermediates in biological proton-coupled electron transfer: A tyrosyl radical prior to proton movement. *Proc. Natl. Acad. Sci. U.S.A. 100*, 8732–8735.

BI801032K